AEROACOUSTIC AND AERODYNAMIC INTERACTION EFFECTS BETWEEN EVTOL
ROTORS

By

GUSTAVO RESENDE COELHO

A THESIS PRESENTED TO THE GRADUATE SCHOOL
OF THE UNIVERSITY OF FLORIDA IN PARTIAL FULFILLMENT
OF THE REQUIREMENTS FOR THE DEGREE OF
MASTER OF SCIENCE

UNIVERSITY OF FLORIDA

2023

To Carla (mom), André (dad), and Diogo (brother)

ACKNOWLEDGMENTS

TABLE OF CONTENTS

LIST OF TABLES

LIST OF FIGURES

LIST OF ABBREVIATIONS

BPF	Blade passage frequency
CFD	Computational fluid dynamics
dB	Decibels
eVTOL	Electric Vertical Take Off and Landing
FFT	Fast Fourier transform
FMM	Fast multipole method
FWH	Ffowcs-Williams and Hawkings
GB	Gigabyte
LE	Leading edge
OASPL	Overall sound pressure level
RAM	Random-access memory
RPM	Rotations per minute
SPL	Sound pressure level
sUAS	Small unmanned aerial systems
TE	Trailing edge
UAM	Urban air mobility
UPM	Unsteady panel method
VPM	Vortex particle method

Symbols

$\vec{u}$	Velocity vector
$\overrightarrow{u_\phi}$	Irrotational velocity contribution
$\overrightarrow{u_\psi}$	Solenoidal velocity contribution
Γ	Vortex ring intensity

ρ	Free-stream mass density
c_T	Coefficient of thrust
R	Rotor radius
θ_{tilt}	Angle of tilt of 5-blade front rotor (tilter)
U_∞	Free-stream velocity
Φ	Azimuthal angle
θ	Elevation angle

Abstract of Thesis Presented to the Graduate School
of the University of Florida in Partial Fulfillment of the
Requirements for the Degree of Master of Science

AEROACOUSTIC AND AERODYNAMIC INTERACTION EFFECTS BETWEEN EVTOL
ROTORS

By

Gustavo Resende Coelho

May 2023

Chair: Steven A. E. Miller
Major: Aerospace Engineering

Electric vertical take-off and landing (eVTOL) aircraft are characterized by their

unconventional wing and electric rotor configurations, which involve both side-by-side

and tandem rotor configurations. These configurations create unique aerodynamic and

aeroacoustic flow-fields. We numerically investigate the interaction effects between

rotor pairs as well as their individual and combined acoustic radiation. We examine

horizontal rotor spacing, rotor tilt angles, and forward flight effects. Performance is

characterized by thrust coefficient, sound pressure level (SPL) at the blade passage

frequency (BPF), and overall sound pressure level (OASPL). This study is performed

with a mid-fidelity aerodynamic solver, DUST, which is used to predict the aerodynamic

flow-field. The tonal acoustic pressure at observer positions is predicted via the

Farassat F-1A formulation of the Ffowcs-Williams and Hawkings equation utilizing the

aerodynamic flow-field. The configurations studied show strong aerodynamic interaction

effects in thrust, as well as out-of-plane acoustic radiation from the aft rotor. Predictions

of thrust and noise are validated via experimental measurement. As rotor separation

decreases, we observe that aft rotor thrust decreases and BPF SPL increases. The most forward rotor, however, is marginally impacted by the interactions.

CHAPTER 1
INTRODUCTION

In recent years, the aerospace industry has seen an increase in the demand for the use of electric motors and propellers to drive propulsors across a range of different vehicle technologies [1]. Examples of such applications are Urban Air Mobility (UAM) and small Unmanned Aircraft Systems (sUAS), which have come a long way from being solely a concept to a near-term reality. The ultimate goal of these systems is to provide an affordable and environmentally friendly solution to transportation within densely populated areas. This would allow for many desirable outcomes, such as traffic relief within cities, quicker cargo deliveries, and quick suburban-urban area transportation [2]. However, these developments still require much progress in order to operate safely and effectively around people.

When anticipating the addition of more aircraft technologies to urban areas, noise is one of the most commonly raised concerns by the general public. In fact, low-noise emission is a key design requirement for urban air vehicles set by governmental agencies [3]. Having said that, the ability to predict and understand how different vehicle configurations generate and emit sound to their surroundings becomes of great importance to designers. This current study investigates how different configurations of electric Vertical Take-Off and Landing (eVTOL) vehicles, a specific class of UAM vehicles, may reduce their generated noise without negatively impacting their performance. Dozens of multimillion-dollar companies like Archer Aviation, Joby Aviation, and Lilium, are in the final design stages of their eVTOL vehicles, as they are now looking to receive certification from governmental agencies in order to begin market operations.

Unlike current operating rotorcraft designs, such as helicopters, UAM vehicles tend to have more complex configurations. For instance, instead of a single main rotor and a tail rotor, these new configurations rely on multiple smaller rotors, and sometimes a fixed wing, in order to generate their necessary lift [1]. Figure 1-1 illustrates four different proposed eVTOL designs with different configurations. The aerodynamic and acoustic characteristics of the aircraft are likely directly related to how the rotors are distributed around the fuselage and the wings. These characteristics may be negatively affected by the aerodynamic interactions between the wakes from each of the rotors, and the rest of the aircraft body. These interactions could result in a significant generation of unwanted noise, both tonal and broadband noise.

(a) Midnight by Archer Aviation

(b) S4 by Joby Aviation
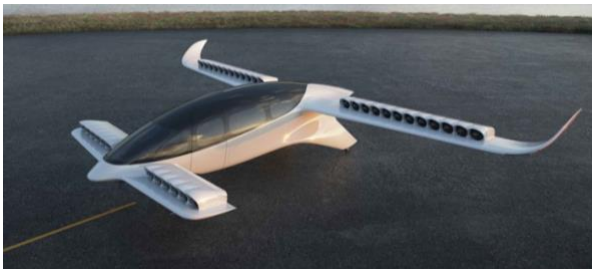
(c) Lilium Jet

(d) Vahana by A[3] by Airbus

Figure 1-1. Examples of different eVTOL designs and configurations: (a) Midnight by Archer Aviation [4], (b) S4 by Joby Aviation [5], (c) Lilium Jet [6], (d) Vahana by A[3] by Airbus [7].

Although isolated propellers have been studied for decades, there has been a lack of studies that capture the full range of flight conditions experienced by one of

these UAM vehicles. In a typical eVTOL design, flight conditions involve ascend, hover, edgewise flight, and forward flight. Edgewise flight, which is characterized by a propeller having a small incident angle to the free-stream flow, is where studies have lacked the most attention [8]. This is particularly important as edgewise flight conditions directly impact the acoustic and force trends in low tip speed rotors with high advance ratios, which is the case for UAM rotors [8]. Additionally, there is a need to understand how rotor-rotor aerodynamic interaction is affected by edgewise flight conditions, and whether this phenomenon is aggravated by different flight conditions.

In recent years, some research studies have been conducted to investigate both the aerodynamic and aeroacoustic characteristics of multi-rotor aircraft. For instance, the work by Healy et al. [9] investigated interactional effects between two rotors, in tandem configuration, in line with the flow. The work was done using high-fidelity computational fluid dynamics (CFD), and it involved nine different rotor separation configurations, both in the vertical and horizontal axes. The study showed how this separation between the rotors can worsen or alleviate the noise problem while impacting the amount of thrust generated by the system. A similar study was conducted by Jia and Lee [3], but in this case, the rotors were set up in a side-by-side configuration using different overlapping separation distances. This work shows, by using high-fidelity CFD, that rotor overlap in this configuration does not drastically impact the emitted overall sound pressure level, but its radiation patterns to differ highly.

Moreover, Misiorowski et al. [10] used high-fidelity CFD to simulate quadcopters operating in cruise using two different configurations: a plus and a cross configuration. The study reports noticeable differences between the two configurations, mostly due to

the interaction between the side rotors and the upwash of the front rotor wake. The study by Duivenvoorden et al. [11] has also reported a similar occurrence, once examining the interactional aerodynamic effects between rotors in ground effect.

Despite these efforts, literature still lacks a certain type of study focusing on the aerodynamic and aeroacoustic interaction effects of eVTOL rotors in the different flight conditions proposed by the many companies looking to go to market. Therefore, this particular study will explore the interaction between rotors in tandem configuration under different free stream conditions, while adjusting the rotor offset spacing, with the goal to find a quiet yet high performance configuration for these types of systems.

Computational fluid dynamics is often used in the design stages of a vehicle, as it provides a viable method of testing and investigating different configurations without having large monetary costs, such as manufacturing and assembling costs. On the other hand, CFD often requires large computational power, which often comes in the form of long simulation times and large monetary costs. High-fidelity CFD simulations, which have been used extensively in this field, such as in the work by Jia et al. [3], have proven to require a large computational effort, which is not suitable for systematic studies of different configurations and test conditions for eVTOL rotor-rotor interactions. Popular high-fidelity codes used for rotorcraft applications include elsA [12] by ONERA, FLOWer by DLR and Airbus [13], and HBM3 [14] by the University of Glasgow. Instead, mid-fidelity CFD, which combines different models, is a great alternative to provide time-accurate simulations with lower computational efforts. This allows for the capture of extensive parametric data that explores the interaction behavior between the rotors

under a comprehensive range of tests, without requiring the same computational resources [15].

Over the past years, several mid-fidelity CFD solvers have been developed for rotary wing applications with the aim of further exploring and understanding rotorcraft aerodynamics. One example of such a tool is the unsteady panel method (UPM) aerodynamic solver, developed by DLR's Institute of Design Aerodynamics [16]. This code was developed for the aeroacoustic simulation of helicopters, using a 3D unsteady free-wake panel method approach to simulate the flow field in addition to a Ffowcs-Williams Hawkings (FWH) based aeroacoustic solver. The vortex particle method (VPM) [17] was used to model the wake, allowing for a visual representation of the aerodynamic interactions between several bodies. Given these features, UPM has also been successfully used by researchers in complex configuration applications, such as eVTOL, in order to simulate the interacting flow-fields of multi-rotor aircraft [18].

Much like UPM, other medium-fidelity CFD solvers were developed focusing on simulating flow around complex UAM configurations to satisfy the market demand for an affordable and reliable solution. DUST, an open-source medium fidelity code developed by Politecnico di Milano in collaboration with A^3 by Airbus [19], is an example of a novel mid-fidelity CFD code. This tool aims to provide designers with fast and reliable results, and it does this by combining different aerodynamic simulation techniques: thick surface panels, thin vortex lattices, lifting lines, and VPM [19]. DUST has been thoroughly validated against wind-tunnel data and high-fidelity CFD solvers, proving to be a good solution for acquiring data on the performance and flow physics of complex eVTOL designs. For instance, DUST has been used to simulate the aerodynamics of the full

Vahana vehicle (displayed in Figure 1-1 (b)), developed by A^3 by Airbus, and showed

good agreement with test flight and high-fidelity CFD data [20]. Having said that, it is

possible to regard DUST as a mature tool to explore the different interactional

aerodynamic effects of complex UAM rotor configurations to further understand and

develop these vehicles.

In the present paper, a combination of DUST and an FWH based aeroacoustic

solver is validated and used to study the aerodynamic and aeroacoustic interactional

effects between a pair of rotors in a tandem configuration – rotors in line with the flow.

This thesis aims to achieve the following objectives:

- Validate and highlight the significance of using mid-fidelity tools, like DUST, in systematic studies and preliminary design. Limitations of said tools will also be discussed.

- Provide a comprehensive investigation of rotor-rotor aerodynamic interaction by means of mid-fidelity numerical simulations, under a series of standard flight conditions experienced by an eVTOL vehicle during its flight, specifically during take-off and landing procedures.

- Address limitations of certain rotor configurations, and provide insights into how the aircraft's performance and stability can be improved.

- Help accelerate the development of eVTOL aircraft and enable the design of more efficient and safe vehicles.

This paper is organized in the following manner. Chapter 2 will outline the

numerical approach implemented in DUST and the acoustic solver code, and describe

the process for determining an appropriate mesh for the rotor blades. Chapter 3 will

describe the validation method used and provide a brief overview of the experimental

setup used to acquire the data. Chapter 4 will present the test cases and flight

conditions chosen for the study. The main aerodynamic and aeroacoustic results

18

acquired will be presented and discussed in Chapter 5. Lastly, conclusions are drawn in

Chapter 6 along with a scope of future work.

CHAPTER 2
NUMERICAL METHOD

Two numerical tools are used in this research study in order to simulate the aerodynamic and aeroacoustic behaviors of the rotors in discussion: DUST and an aeroacoustic solver developed by our research group. Figure 2-1 displays a flow-chart of the entire prediction system employed. This chapter will be split into three different sections for clarity: the aerodynamic tool, the aeroacoustic tool, and the surface mesh generation methodology.
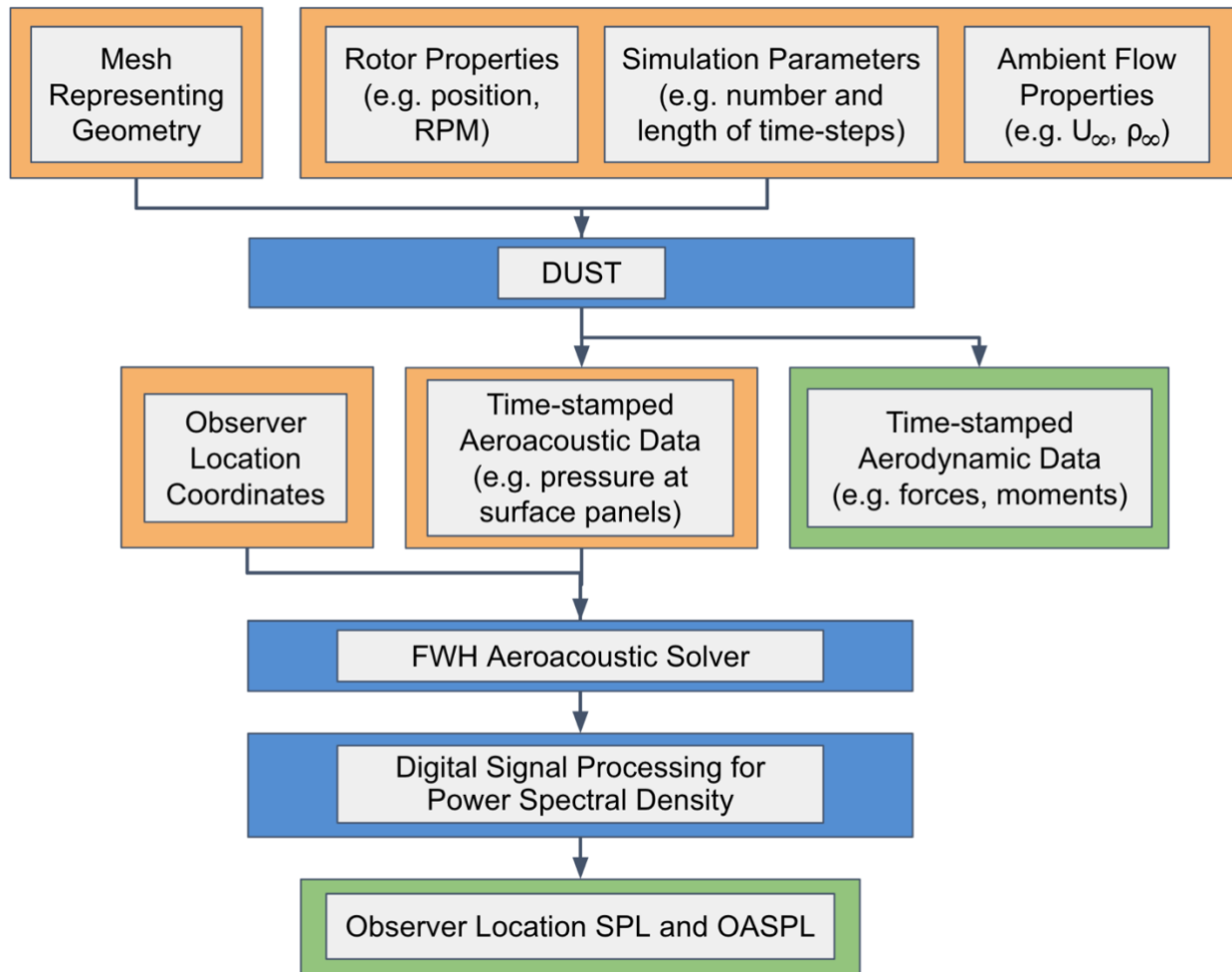

Figure 2-1. Flow-chart of the prediction system. Boxes in orange highlight the inputs, blue boxes highlight the processes, and green boxes highlight investigated outputs.

2.1 DUST

As mentioned previously, DUST is a flexible aerodynamic tool that allows for the flow simulation of models of different complexities. Its goal is to promote a fast and reliable method of obtaining the aerodynamic flow-field around bodies involving complex configurations, such as novel eVTOL aircraft designs. It achieves this by modeling 3D bodies using the combined integration of thick surface panels, thin vortex lattices, and lifting lines while modeling the wake using panels and vortex particles [15]. A crucial aspect of DUST is its ability to simulate interactional aerodynamics phenomena, which is done using a Fast Multipole Method (FMM) [21]. This is particularly important in this study as the interaction between multiple bodies and wakes can be observed. DUST is based on the Helmholtz decomposition of the velocity field, $\vec{u} = \vec{u_\phi} + \vec{u_\psi}$, where $\vec{u_\phi}$ and $\vec{u_\psi}$ are the irrotational and solenoidal velocity contributions, respectively. The solver's algorithm progresses its solution through time steps by alternating between a three-dimensional boundary element method for $\vec{u_\phi}$ and the Lagrangian evolution in time for $\vec{u_\psi}$ [15].

The object being investigated is defined through a surface mesh, which is composed of different elements depending on the level of fidelity required. The aerodynamic elements used are lifting lines, zero-thickness lifting surfaces, and surface panels. A piecewise-uniform distribution of doublet and sources is used to create the surface panels, while the lifting lines are constituted by a vortex ring along with trailing vortices [15], [22]. In the case of a high aspect ratio body, like a rotor blade, the body is modeled by one-dimensional lifting line elements that include viscous effects modeling. The lifting line strength is defined by the vortex ring intensity, Γ, which is calculated

through a nonlinear algorithm that takes into account the different aerodynamic

coefficients (e.g. lift, drag, and pitching moments) of the lifting sections [15]. Having said

that, DUST relies on the combination of the Γ-method and a α-method, which are

$$\frac{1}{2}\rho|U_{rel,i}|^2 c_i c_{l,i}\big(\alpha_i(\Gamma_k)\big) = -\rho|U_{rel,i}|\Gamma_i,$$
(2-1)

and $\quad \alpha_i = \operatorname{atan} 2(U_{rel,i}(\alpha_k)\cdot\hat{n}_i, U_{rel,i}(\alpha_k)\cdot\hat{t}_i),$
(2-2)

where ρ is the free-stream density, $U_{rel,i}$ is the relative velocity at the control point of the

i^{th} section, c_i is the ith section chord, $c_{l,i}(\alpha_i)$ is the lift curve, and α_i is the incident angle.

The control point is calculated at three-quarters of the chord when the lifting line is

located at the quarter chord. Equation 2-1 equates the sectional lift semi-empirical

equation and the Kutta-Joukowski theorem [15]. On the other hand, Equation 2-2

evaluates the two-dimensional aerodynamic coefficients using the incident angle as an

input, which is induced by the different wake components generated by the different

aerodynamic elements (e.g. lifting lines and particles) [22].

    As mentioned previously, DUST's ability to simulate a robust wake shed is critical

for the representation of the interactional aerodynamic effects between different bodies,

such as rotors and wings. This is done using VPM, a Lagrangian grid-free method used

to evaluate the progression of the wake through the rotational component of the velocity

field $\overrightarrow{u_\psi}$, by approximating the vorticity field using vortex particles. By following the

derivation steps described by Piccinini et al. [15], we obtain the contribution of velocity

induced by the particles, as follows,

$$\vec{u}_\psi^h(\vec{r},t) = \sum_{p=1}^{N_p}\vec{K}^h\left(\vec{r}-\vec{r}_p(t)\right)\times\overrightarrow{\alpha_p}(t),$$
(2-3)

where $\vec{r}_p(t)$ is the position, $\overrightarrow{\alpha_p}(t)$ is the intensity, N_p is the number of particles, and $\vec{K}^h$ is

the discrete kernel given by the Rosenhead-Moore kernel,

$$\vec{K}^h(\vec{x}, \vec{y}) = -\frac{1}{4\pi}\frac{\vec{x}-\vec{y}}{\left(|\vec{x}-\vec{y}|^2+R_v^2\right)^{\frac{3}{2}}},$$

(2-4)

where R_v is the radius of the vth vortex particle. This kernel fits naturally in the Cartesian FMM, allowing for the evaluation and tracking of the vortex term, which is a function of both vortex intensity and distance between interacting particles [15].

2.2 Ffowcs-Williams Hawkings Solver

Once the flow field is generated using DUST, an aeroacoustic tool is needed to predict the propagation of pressure to the far-field in order to acquire noise levels at particular observer locations. The tool in discussion is an aeroacoustic code based on Farassat's 1A formulation [23], an extension to the Ffowcs-Williams Hawkings equation [24]. The FWH equation is given as follows,

$$\square^2 p' = \frac{\partial}{\partial t}[\rho v_n \delta(f)] - \frac{\partial}{\partial x_i}[p n_i \delta(f)] + \frac{\partial^2}{\partial x_i \partial x_j}\left[T_{ij}H(f)\right],$$

(2-5)

where $\square^2$ is the wave or D'Alembertian operator in 3-D space, p' is the local static pressure, v_n is the flow velocity, $\delta(f)$ is the Dirac Delta function, n_i is a unit vector at the ith surface pointing outward, T_{ij} is the Lighthill's stress tensor, and $H(f)$ is the Heaviside function. We assume p' to be the acoustic pressure when the fluctuations in density are very small compared to the ambient density, i.e. $\frac{\rho'}{\rho_0} \ll 1$. Lighthill's stress tensor is given by,

$$T_{ij} = \rho v_i v_j + p_{ij} - c_\infty^2 \rho \delta_{ij} = \rho v_i v_j + (p - c_\infty^2 \rho) - \tau_{ij},$$

(2-6)

where τ_{ij} is the viscous stress term and c_∞ is the ambient speed of sound [24]. The algorithm for the code takes into account FWH's equation for a penetrable porous source is solved, shown as follows:

$$\Box^2 p' = \frac{\partial}{\partial t}[\rho_0 U_n \delta(f)] - \frac{\partial}{\partial x_i}[L_i \delta(f)] + \frac{\partial^2}{\partial x_i \partial x_j}[T_{ij} H(f)].$$

(2-7)

Here, following notations are used:

$$U_n = \left(1 - \frac{\rho}{\rho_0}\right) v_n + \frac{\rho u_n}{\rho_\infty}$$

(2-8)

$$L_i = p\delta_{ij}n_j + \rho u_i(u_n - v_n)$$

(2-9)

where δ_{ij} is the Kronecker delta function [23]. By evaluating Equation 2-7 as a function of time and observer location, the acoustic pressure in the far-field can be predicted. This is performed using a retarded time algorithm as described by Brentner [25]. All the quantities derived from Equation 2-7 are sampled with various FWH surfaces from DUST calculations and used as input to the acoustic solver. The surface panels from the aerodynamic solver are used as the noise sources, hence the face areas, face centers, and face normal are all acquired from the surface mesh from DUST. Using the retarded time algorithm, we march in time at the observer location and calculate the retarded time by tracing the sound signal back to the porous surface. By interpolating quantities to match the sampled CFD time data, the total acoustic pressure fluctuation is calculated by summing all the contributions from each of the porous surfaces, resulting in the total tonal acoustic radiation across time from the turbulent flow-field. Lastly, using a fast Fourier Transform (FFT), digital signal processing for power spectral density is performed in order to process the time-domain data into spectra for analysis and comparison with the experimental data.

2.3 Rotor Blade Surface Mesh Generation

When using DUST, solid body surface meshes can be composed of triangular or quadrilateral surface panels. Although little difference is observed between the two

types, quadrilateral surfaces are used in this study due to their simple connectivity. In order to generate the blade's surface, the length of the blade in the spanwise direction is split into equal-sized partitions, while the length in the chordwise direction is partitioned by different sizes according to a cosine distribution in the leading edge (LE) of the blade. This means that the panels are shorter near the LE in order to better represent the curvature of the geometry of the blade. This choice of distribution is also justified by the results of the mesh size study performed and shown below. This study was performed to find an optimum number of panels in both the chordwise and spanwise directions; the purpose of this is to find an appropriate balance between required computational power and simulation results accuracy. By varying the size of the mesh representing the blade's surface, small changes in thrust and sound pressure level (SPL) at the blade pass frequency (BPF) were observed in comparison to a high-definition mesh, referenced as the base case, which is considered the most accurate configuration. It is important to note that this study was performed using a single 2-blade rotor in a three-dimensional domain, instead of the dual rotor configuration presented in the later chapters of this paper. Below are the results of this study:
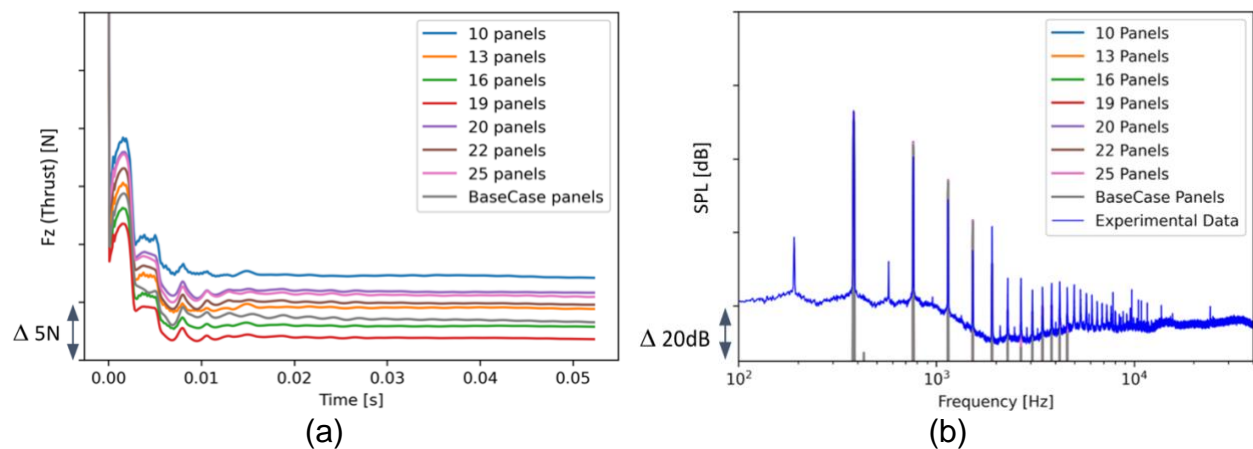

Figure 2-2. Spanwise mesh size study for both (a) thrust and (b) SPL.
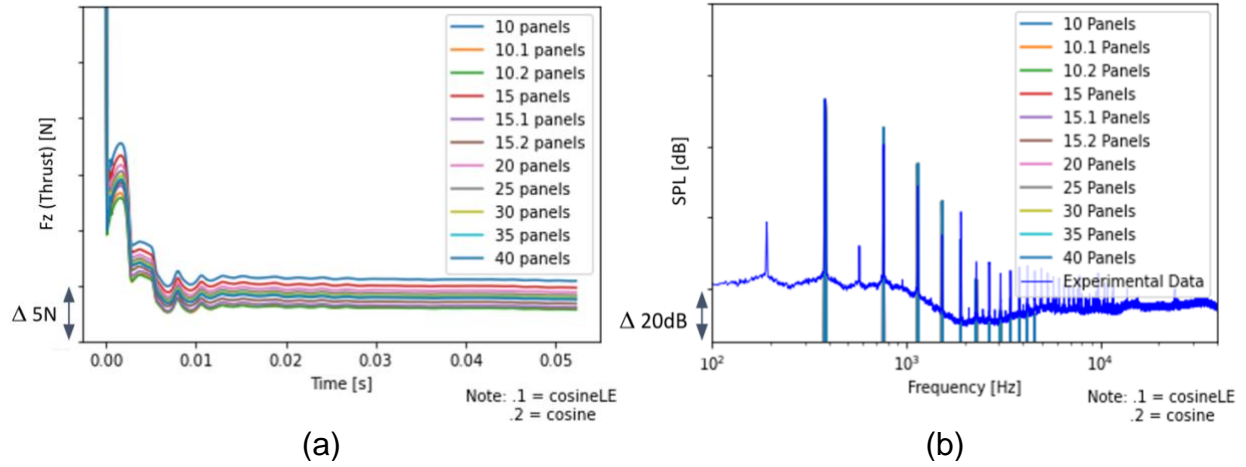
Figure 2-3. Chordwise mesh size study for both (a) thrust and (b) SPL at BPF.

Table 2-1. Values for Δc_T and ΔdB with respect to the base case acquired from both the mesh size studies

Spanwise			Chordwise		
Number of Panels	Thrust (Δc_T)	SPL (ΔdB)	Number of Panels	Thrust (Δc_T)	SPL (ΔdB)
10	0.141	0.9778	10	0.073	0.0186
13	0.027	0.9772	10 (cosine LE)	-0.031	-0.0182
16	-0.038	0.9794	10 (cosine)	-0.034	0.4589
19	-0.080	0.9854	15	0.050	0.0186
22	0.088	0.9351	15 (cosine LE)	-0.023	-0.0182
25	0.046	0.9261	15 (cosine)	-0.011	0.4589
			20	0.031	0.0186
			25	0.019	0.0186
			30	0.011	0.0186
			35	0.008	0.0186
			40	0.004	0.0186

The figures and table above show a correlation between the number of panels and the accuracy of results, which is expected. By varying the number of panels in the spanwise direction, it is possible to observe a change of up to 6.5% in thrust and 7% in SPL at the blade pass frequency; BPF is defined as

$$BPF = \frac{n\Omega}{60},$$ (2-10)

where n is the number of blades and Ω is the rotation rate (rotations per minute). Now, for the chordwise direction, it is possible to observe a change of up to 7% in thrust, but negligible change in SPL at the blade pass frequency. When considering the different values along with their respective simulation run times, a mesh size of 13 panels (with a cosine LE distribution) in the chordwise direction and 25 panels in the spanwise was chosen. These values account for only one of the faces of the rotor blade, therefore, each blade has 13x25 panels on its top surface and 13x25 panels on its bottom surface. With this configuration, the computational time of the simulation of the dual rotor setup was approximately 45 minutes while using a workstation running a single-processor 11th generation Intel Core i7-11700K at 3.60 GHz with 32 GB of RAM. Figure 2-4 below shows the mesh used to represent the 2-blade rotor.
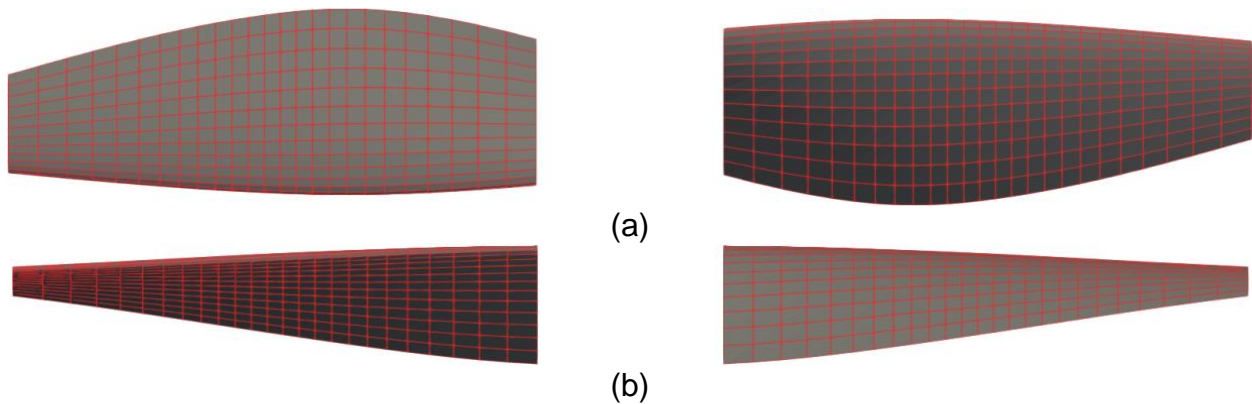

(a)

(b)

Figure 2-4. Mesh used to represent the 2-blade rotor; shown are (a) the top view and (b) the front view. Each surface is composed of 13x25 panels, and panels are placed using a cosine LE distribution in the chordwise direction.

CHAPTER 3
VALIDATION OF NUMERICAL METHOD

A validation study was performed by comparison with experimental data acquired from the University of Florida's anechoic wind tunnel. The data considered was obtained by Goldschmidt and Tingle [26] in a collaboration with Archer Aviation, using a sub-scale rotor model of Archer's Maker aircraft. Figure 3-1 shows the experimental setup with the dual rotor configuration in place.
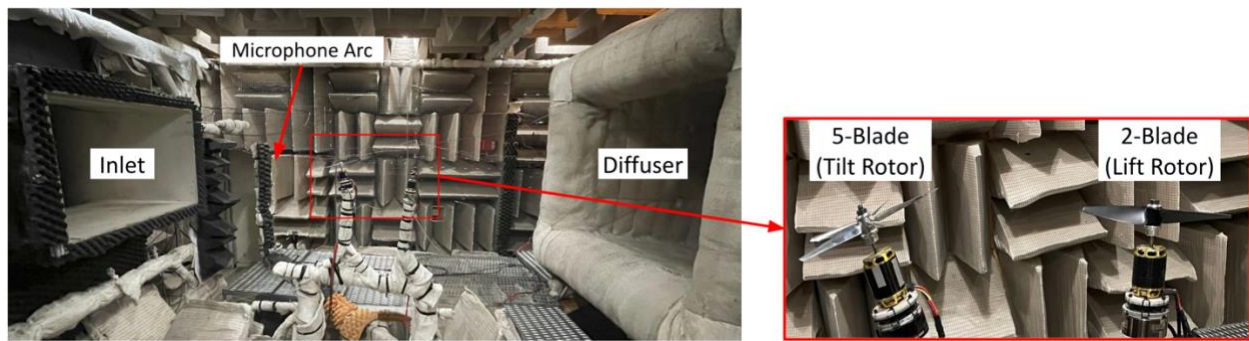
Figure 3-1. University of Florida's anechoic wind tunnel with the dual rotor in tandem configuration set up [26].

A numerical model was developed using the rotor geometry provided by the company using the surface mesh process previously explained. The geometry information made available considered the span, twist, chord ratios, thickness ratios, and sweep of the company's prototype aircraft's 2-blade and 5-blade rotors. For this validation study, three overall cases were conducted: one for each of the isolated rotors (2-blade and 5-blade), as well as one for the dual rotors in tandem configuration. All three cases involved both hover and forward flight conditions. In order to measure the accuracy of the numerical method employed, the coefficient of thrust (c_T), SPL at the BPF, and OASPL will be measured and compared between the two data sets. The equation used for c_T is given as

$$c_T = \frac{\tilde{F}_Z}{\rho (R\Omega)^2 (\pi R^2)},$$

(3-1)

where $\tilde{F}_Z$ is the mean force normal to the rotor (rotor thrust), ρ is the free-stream

density, R is the rotor radius, and Ω is the rotation rate. The time-stamped thrust values

are given by DUST.

From Figure 3-1a, we are able to observe the coefficient of thrust generated by

DUST as a function of time, in two simulations lasting over 0.05 seconds, for the two-

blade rotor. Both of these simulations clearly indicate the moment that their respective

c_T values reach steady state, at a little over 0.03 seconds. This represents the time it

takes for the rotors to generate fully developed wakes, hence this is the desired range

for any calculations regarding the rotor's thrust and acoustics. Although this data range

would be enough to move forward, the simulation duration will be doubled to enable a

larger steady-state sample for the aeroacoustic analysis. This is critical due to the extra

time required for the first rotor's wake to travel downstream to interact with the second

rotor in larger offset cases. This time extension is shown in Figure 3-1b, which displays

the c_T for each of the rotors in the dual rotor configurations during a forward flight case.
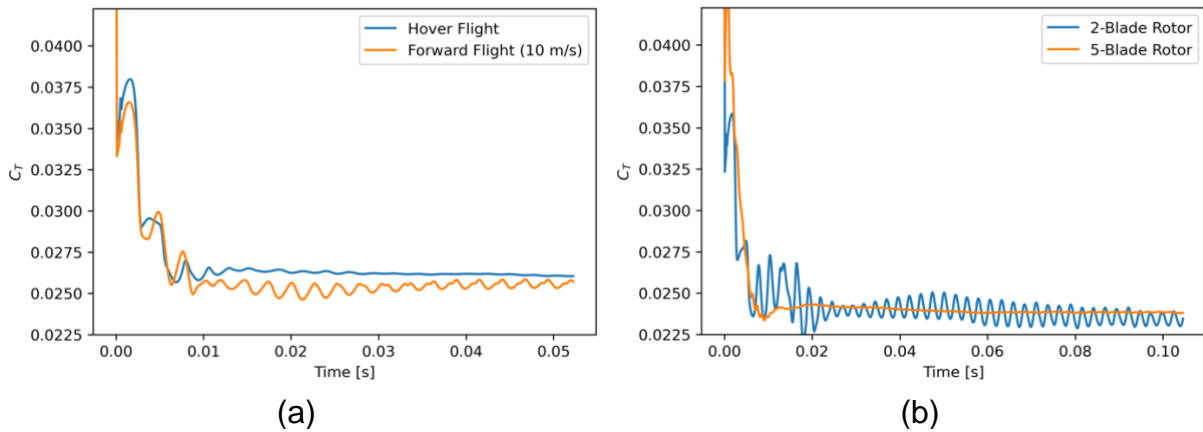

(a)   (b)

Figure 3-2. Time histories of the c_T for three validation cases: (a) 2-blade rotor in hover
and forward flight conditions and (b) dual rotor system in forward flight
conditions.

From the thrust data shown above, we are able to acquire the average C_T values from the steady state range in order to compare them to the experimental data C_T. The DUST simulations are in good agreement with the experimental data, as a small error of $\pm 1\%$ in thrust coefficient is observed in low free-stream velocity (< 15 m/s) flows. However, some discrepancies were observed at higher free-stream velocities, specifically in flows with velocities over 20 m/s. This finding is similar to what has been reported by Piccinini et al. [15] in their validation studies of DUST.

(a)   (b)
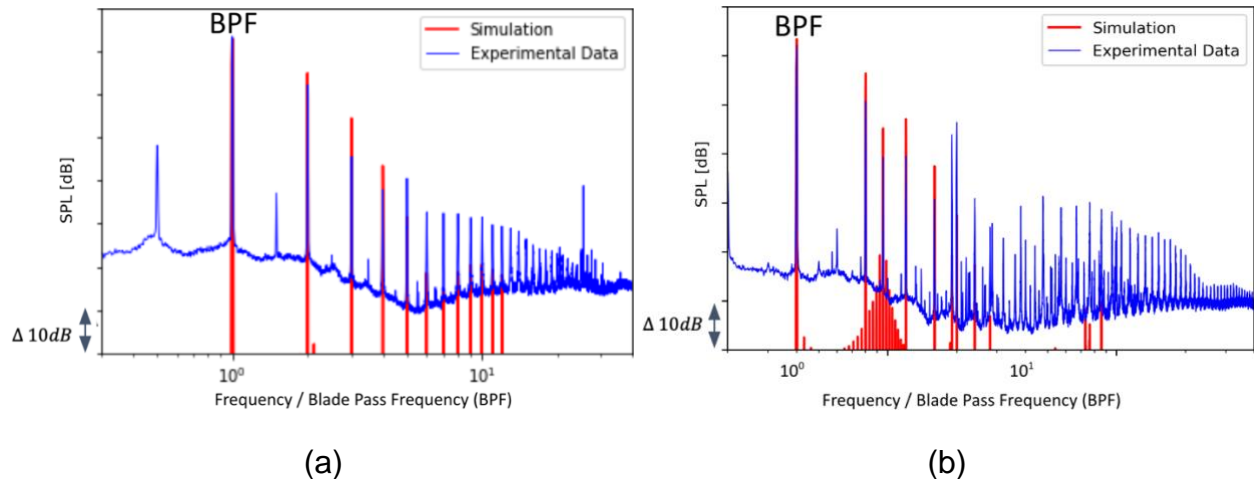
Figure 3-3. Comparison of the sound pressure level (SPL) in the frequency spectra between the simulation and experimental data. (a) 2-blade rotor in hover; (b) and for the dual rotor system in hover. Note: The BPF value indicated in both plots refers to the blade pass frequency of the 2-blade rotor.

Figure 3-3 shows the comparison in SPL between the simulation data acquired using the numerical method described and the experimental data acquired in the wind tunnel; both cases display results from the hover test condition. These frequency spectra were acquired using the steady state range in their respective simulations. It is important to keep in mind that the aeroacoustic solver employed only predicts the tonal acoustics of the system, hence no broadband prediction is made. Additionally, the group

of tones present in the high-frequency region is due to the noise produced by the electric motor in the experimental setup [26], which is not included in the simulations.

The SPL results are in good agreement with the experimental data. In particular, the FHW solver does a good job of predicting noise at the different observer locations in low-speed cases. This is a direct impact of DUST's limitations previously discussed. As shown in the plots, the SPL at the BPF for both cases, along with others, match within 1.5 dB. The OASPL, which is calculated by integrating the SPL data, match within 2 dB in all the cases. In certain cases, the differences between the values are negligible, as SPL at the BPF matches within 0.02 dB and OASPL matches within 0.5 dB.

Having said that, the combination of the aerodynamic and the aeroacoustic tools has generated fairly accurate results. Therefore, they can be considered appropriate for studying the wake interactions between multiple propellers, especially under low free-stream velocity flight conditions.

CHAPTER 4
NUMERICAL MODEL AND TEST CASES

As mentioned previously, this paper studies the aerodynamic and aeroacoustic interactive effects between two sub-scale rotors placed in a tandem configuration. This means both rotors are in line with the free-stream flow, hence the rear rotor stands directly behind the front rotor. This configuration can be observed in a series of different proposed UAM designs, such as the designs shown in Figures 1-1a, 1-1b, and 1-1d. For this study, the configuration will be similar to that of Archer's Marker aircraft, a prototype used for the development of Archer's Midnight (shown in Figure 1-1a). This aircraft design features 12 rotors, in two rows of six; the first row of six is placed in front of the wing's leading edge, while the second row is placed after the trailing edge of the wing. The first six rotors have five blades and are defined as tilter rotors, as they tilt forward in order to produce forward thrust during forward flight. The rear six rotors have two blades and are defined as lifters, as they remain at the same angle throughout all flight configurations to produce upwards lift. Archer's Maker is shown in Figure 4-1a.

(a)   (b)

Figure 4-1. Motivation for the current study's rotor configuration. (a) Archer's Maker aircraft in forward flight configuration during a test flight [4]. Tilter rotors are tilted forward, while lifter rotors are upright. (b) Simplified rotor configuration for the current study is outlined by the red box [26].

The numerical model presented in this study only takes into account the rotor blades, while neglecting any other bodies in the simulation, such as the rotor's hub, electric motor, wing, and rotor booms. This way, we can isolate any interactional effects between these bodies. In this study, three controlled variables are adjusted in order to investigate the rotor-rotor interactions: 5-blade rotor tilt angle (θ_{tilt}), horizontal rotor offset, and free-stream velocity. The tilt angle is measured from the vertical axis to the rotor plane, hence a 0° tilt angle indicates a rotor facing directly into the free-stream flow, while a 90° tilt angle indicates a rotor facing upwards orthogonal to the free-stream flow (hover configuration). The horizontal rotor offset is measured in terms of rotor radii, and it is the distance between the center points of both rotors. Additionally, the rotors diameter, rotation per minute (RPM), and vertical placements are all kept constant across the two rotors during all test cases. It is important to note that both rotors will rotate in the same direction (counterclockwise when viewed from the top) with the same RPM. Figure 4-2 shows a diagram of the numerical model with the important variables labeled.

In order to run test cases where all parameters are adjusted independently, 84 different simulations are performed. From these, 24 simulations are performed using isolated rotors: 12 simulations for the isolated 2-blade lifter and 12 simulations for the isolated 5-blade tilter. The isolated cases are needed to obtain the reference performance for each of the rotors, without having any interaction effects between them. This way, we are able to acquire the different thrust and noise levels for each of the isolated rotors, at all angles and free-stream velocity conditions, for comparison with the interacting dual rotor setup. Also, Table 4-1 highlights all the controlled values studied.

33

Table 4-1. Controlled parameters in the dual rotor configuration

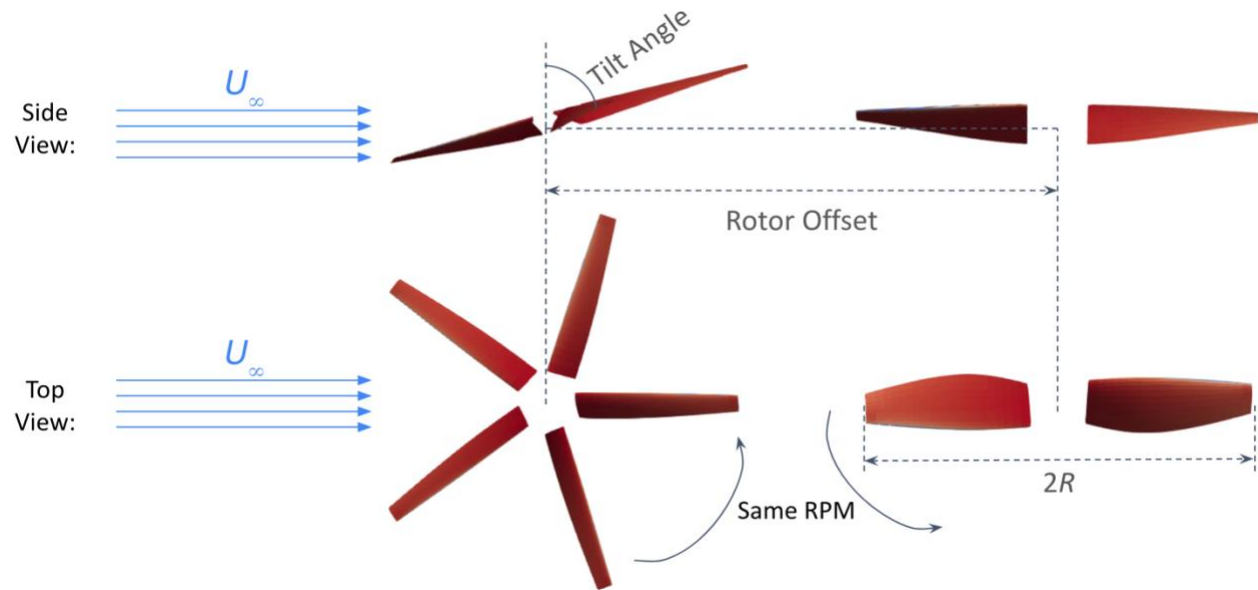| Tilt Angle (θ_{tilt})	Rotor Offset	Free-stream Velocity (U_∞)
60°, 70°, 80°, 90°	2.5R, 3R, 3.5R, 4R, 4.5R	0 m/s, 5 m/s, 10 m/s

Figure 4-2. Side and top views of the numerical model used in DUST, with labeled rotor offset, free-stream velocity U_∞, and tilt angle parameters.

Four different far-field observer locations are used for the aeroacoustic analysis. All of these are located at the same azimuthal angle at a distance of 8.5R from the mid-point between the two rotors, on their advancing side. This mid-point does not change between predictions. Starting with the first observer location at the rotor plane, each subsequent observer is moved downwards 10° respectively relative to the horizontal plane, while keeping the same distance. Figure 4-3 shows this observer location distribution, where Φ is the azimuthal angle in degrees and θ is the elevation angle in degrees.

It is important to note that the shown observer locations, tilt angles, and low velocities were all chosen to simulate take-off and landing conditions. This specific

range of flight condition is important to be thoroughly understood as the public is exposed to it the most, due to a vertiport's location and expected high frequency of flights [2].
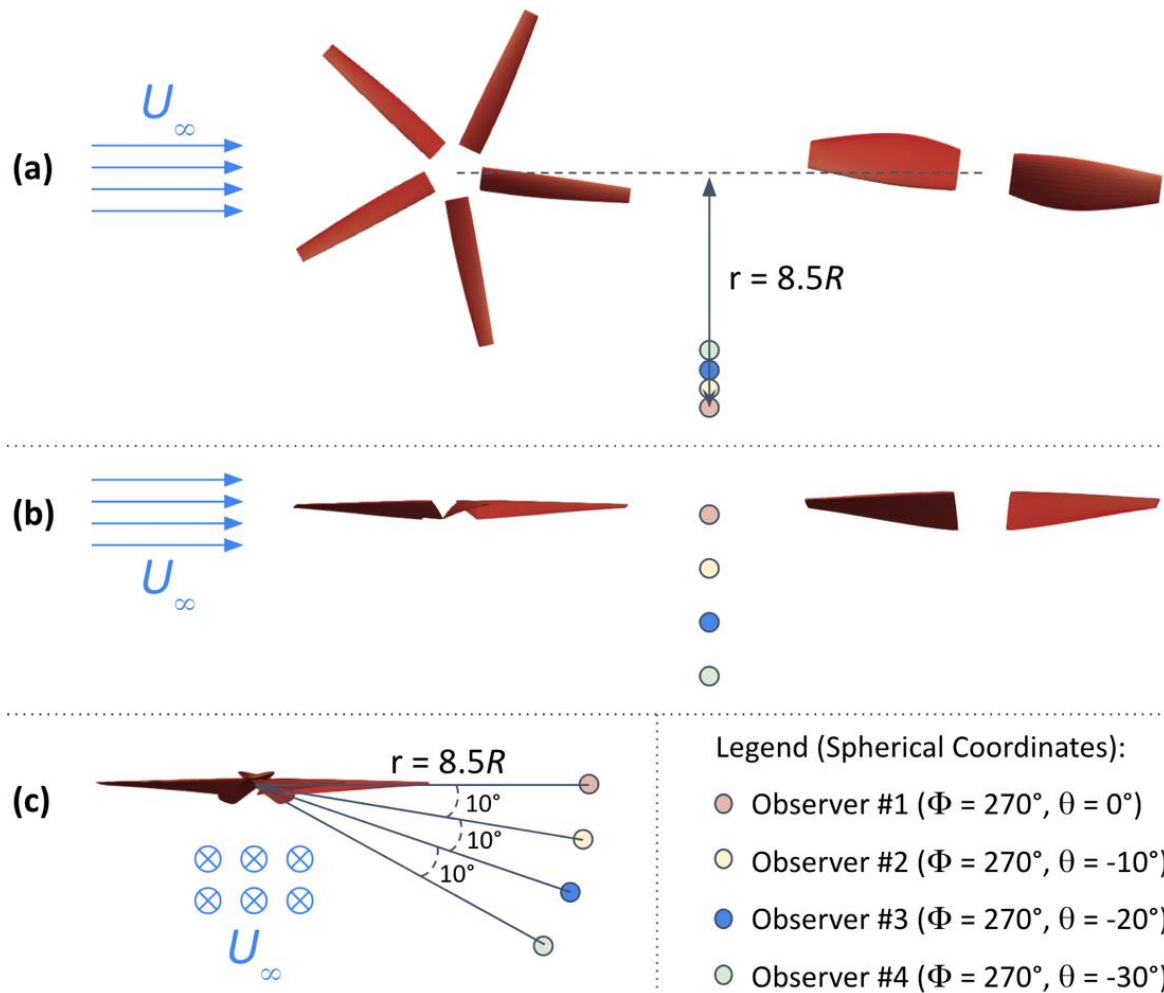

Figure 4-3. Acoustic observer locations used in the aeroacoustic analysis; distance not drawn to scale. (a) Top view, (b) side view, (c) front view of the system.

CHAPTER 5
RESULTS AND DISCUSSION

This section will highlight the main results obtained from the tandem dual rotor simulations performed. The goal of this chapter is to discuss the differences between the isolated rotor cases and the dual rotor interactive cases, by a means of comparing the performance of both. Ideally, these results would present an optimal vehicle configuration to minimize noise generated while maximizing thrust from both rotors. This chapter will be split into three components: qualitative wake analysis, thrust analysis, and acoustic analysis.

5.1 Wake Results

Figures 5-1 and 5-2 show the comparison of the fully developed wakes of the dual rotor systems with the combined isolated rotors' wakes. A couple of flight conditions are used to illustrate all of the study's results, each featuring distinct rotor offsets ($2.5R$ and $4.5R$). The first condition is at hover ($\theta_{tilt} = 90°$) with $U_\infty = 0$ m/s, while the second condition is forward flight ($\theta_{tilt} = 60°$) with $U_\infty = 0$ m/s. These comparisons are interesting as the hover case is expected to have a low interactive behavior, while the forward flight case has a high interactive behavior due to the free-stream flow and tilt rotor's thrust pushing its wake backward.

Additionally, these figures show how the two rotors' wakes interact with one another, and how the distance between them impacts their spreading and vertical reach. As shown, the wakes from both rotors develop fairly unaffected for a distance of about $2R$; however, after this range, the wakes from Figures 5-1a and 5-2a begin to affect each other due to the low-pressure region between them. This forces the wake particles to move into the gap between the rotors' wakes, impacting their respective

36

spreads, resulting in the wake becoming wider and shorter. In comparison with the isolated rotors' wakes, it is possible to observe a wake height reduction of about $2R$ and $3.75R$ for the tilter rotor and lifter rotor, respectively. On the other hand, in Figures 5-1b and 5-2b, it is possible to observe less interaction between the wakes, resulting in small differences between the isolated and dual rotor configurations' wakes. For this case, we can once again observe the wakes becoming wider due to the low-pressure region between the two rotors, however, that does not seem to impact the height of the wakes as much. It is important to keep in mind that both rotors are spinning in the same direction, hence the two wakes oppose each other when they meet in the middle, causing interactive effects between them.

Similarly, Figures 5-3 and 5-4 show how the two wakes interact with one another, but now, in a typical forward flight configuration. Here, due to the flight conditions, the interaction between the rotors' wakes is hard to avoid, regardless of the rotor offset. However, as the rotor offset increases, the interactive behavior seems to worsen. The lower boundary of the wakes in Figures 5-3a and 5-4a are much smoother than those of Figures 5-3b and 5-4b, overall resulting in a more accurate match to the shape of the wake from the isolated cases. Additionally, it is possible to observe that as the rotor offset increases, there is more room for the wake from the front rotor to climb and enter the low pressure region that feeds air into the aft rotor's disk, impacting the 2-blade rotor's wake and performance.

The four cases shown in Figures 5-1 through 5-4 do a good job of summarizing the overall behavior between the wakes. In flight conditions similar to hover, a larger rotor offset results in fewer interactions between the wakes. However, in flight

conditions that force interactions between the rotors (e.g. tilting rotor, high free-stream velocities), a larger rotor offset is not always desirable, due to the turbulent wake feeding into the aft rotor's inlet region. This issue could be potentially mitigated by the addition of a large body (e.g. wing) between the rotors, but this is not explored in this current study.

<p style="text-align:center">(a)   (b)</p>

Figure 5-1. Qualitative wake comparison between dual rotor system's wake (blue) and isolated rotors' wakes (yellow) at hover ($\theta_{\mathrm{tilt}} = 90°$ with $U_\infty = 0$ m/s), from a side view. Each point corresponds to a wake particle. The rotor on the left is the 5-blade tilter and the rotor on the right is the 2-blade lifter. Their rotor offsets differ as follows: (a) offset = $2.5R$, (b) offset = $4.5R$.
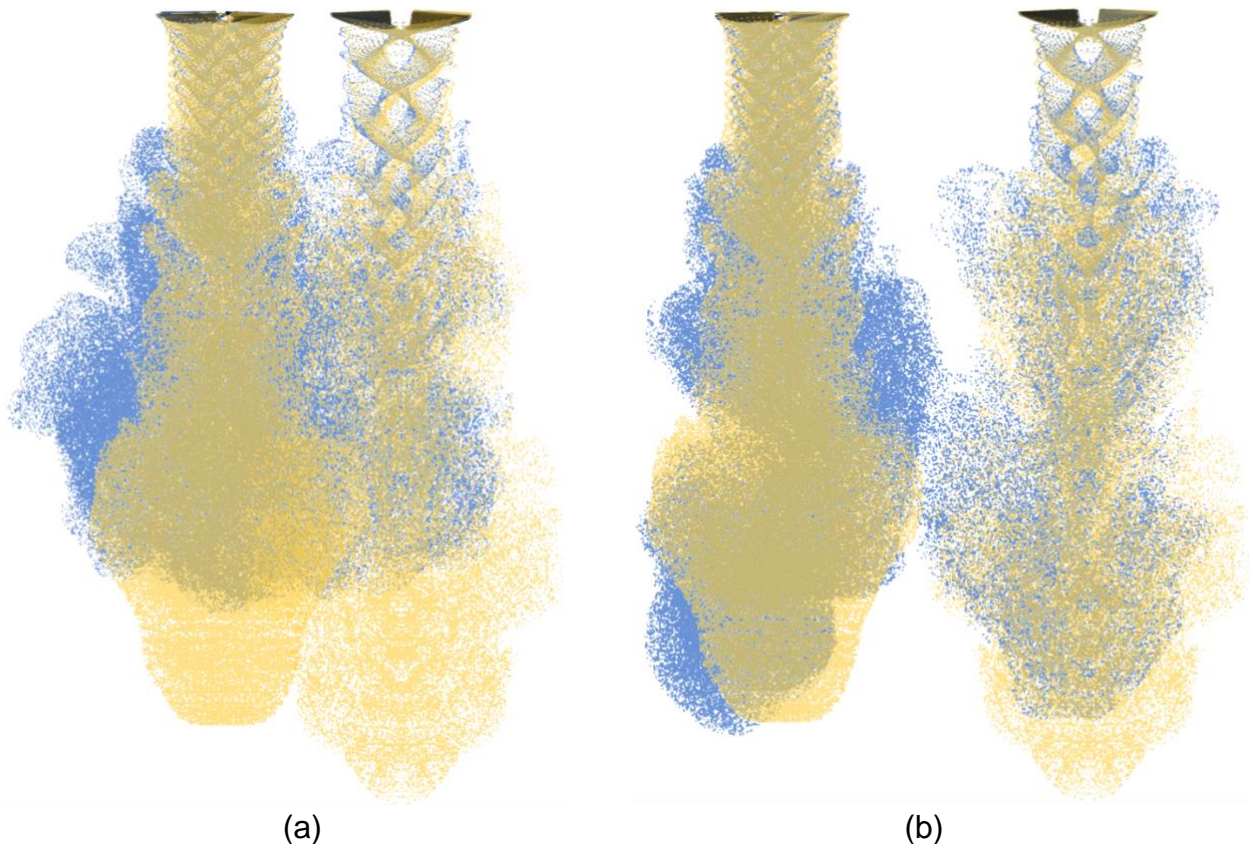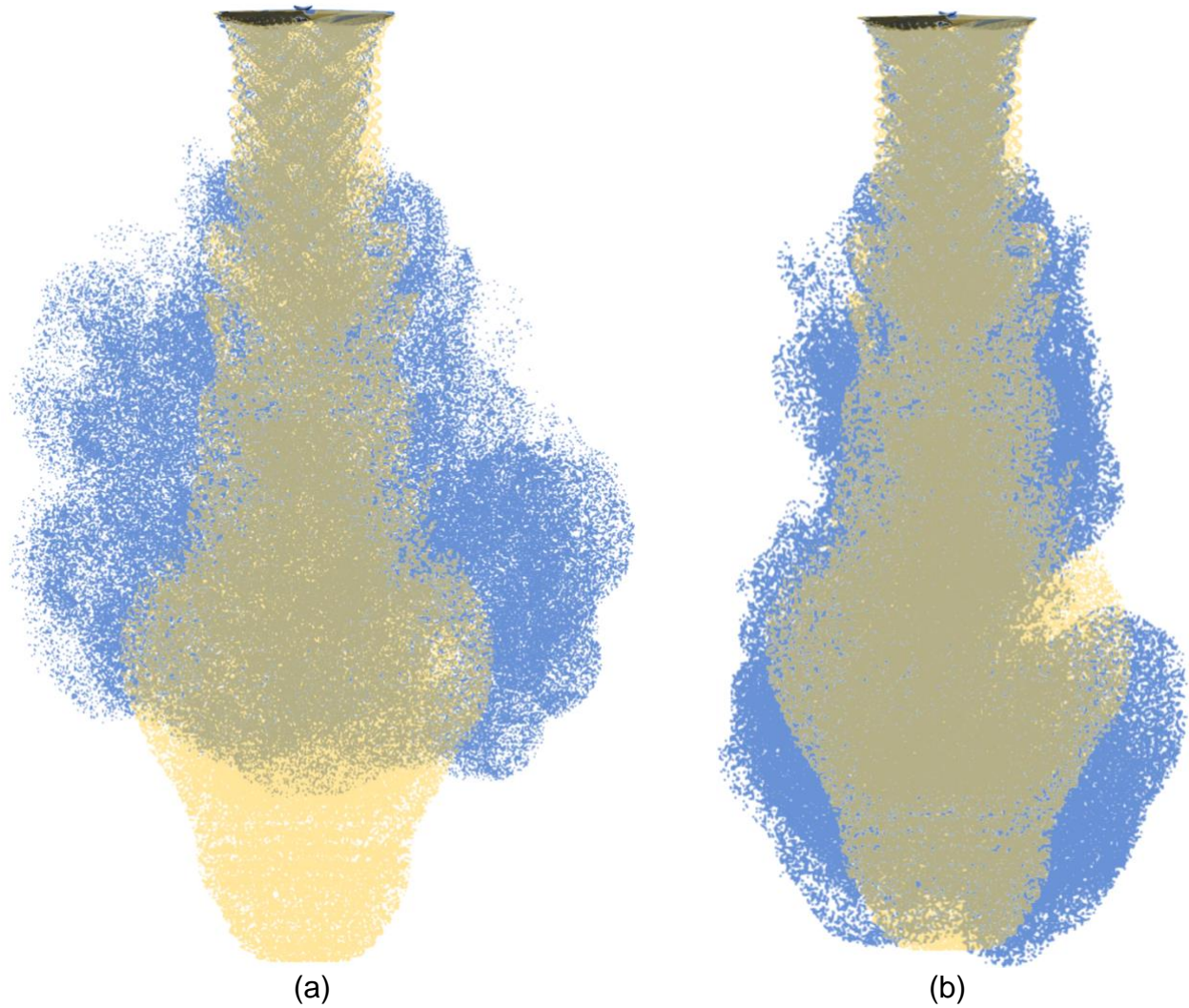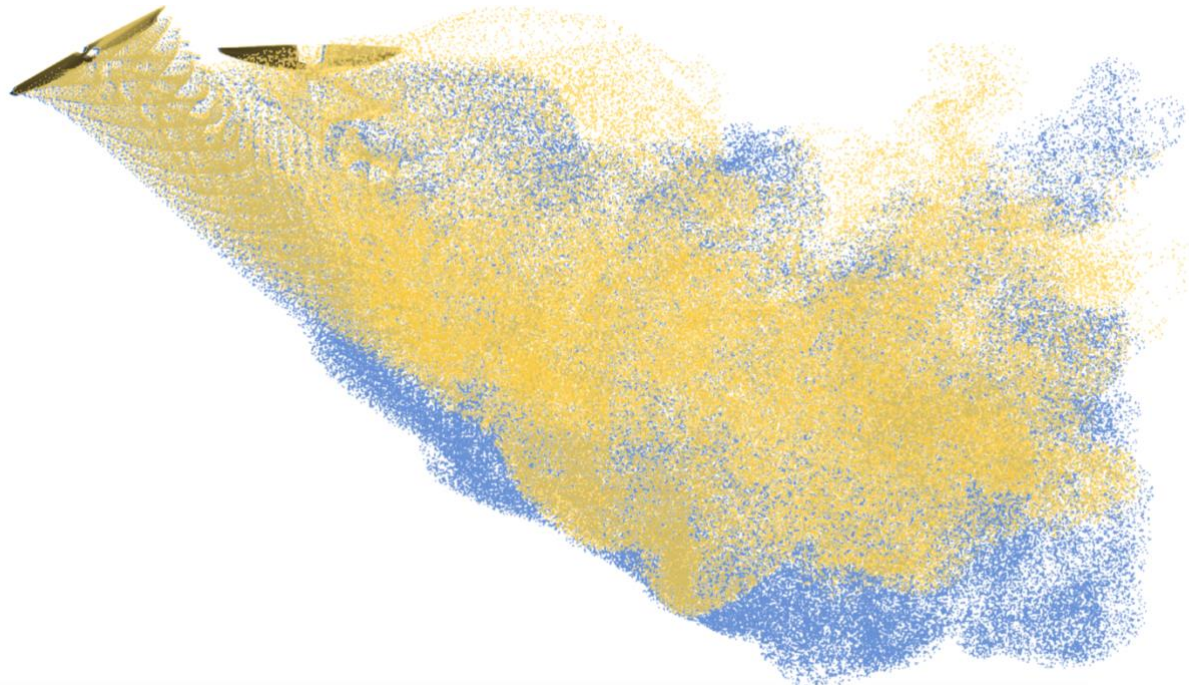
Figure 5-2. Qualitative wake comparison between dual rotor system's wake (blue) and isolated rotors' wakes (yellow) at hover ($\theta_{\text{tilt}} = 90°$ with $U_\infty = 0$ m/s), from a front view. Each point corresponds to a wake particle. Their rotor offsets differ as follows: (a) offset = $2.5R$, (b) offset = $4.5R$.

(a)

(b)

Figure 5-3. Qualitative wake comparison between dual rotor system's wake (blue) and isolated rotors' wakes (yellow) at a forward flight case ($\theta_{\text{tilt}} = 60°$ with $U_\infty = 10$ m/s), from a side view. Each point corresponds to a wake particle. The rotor on the left is the 5-blade tilter and the rotor on the right is the 2-blade lifter, and the freestream flow is moving from left to right. Their rotor offsets differ as follows: (a) offset = 2.5R, (b) offset = 4.5R.

<p style="text-align:center">(a)   (b)</p>

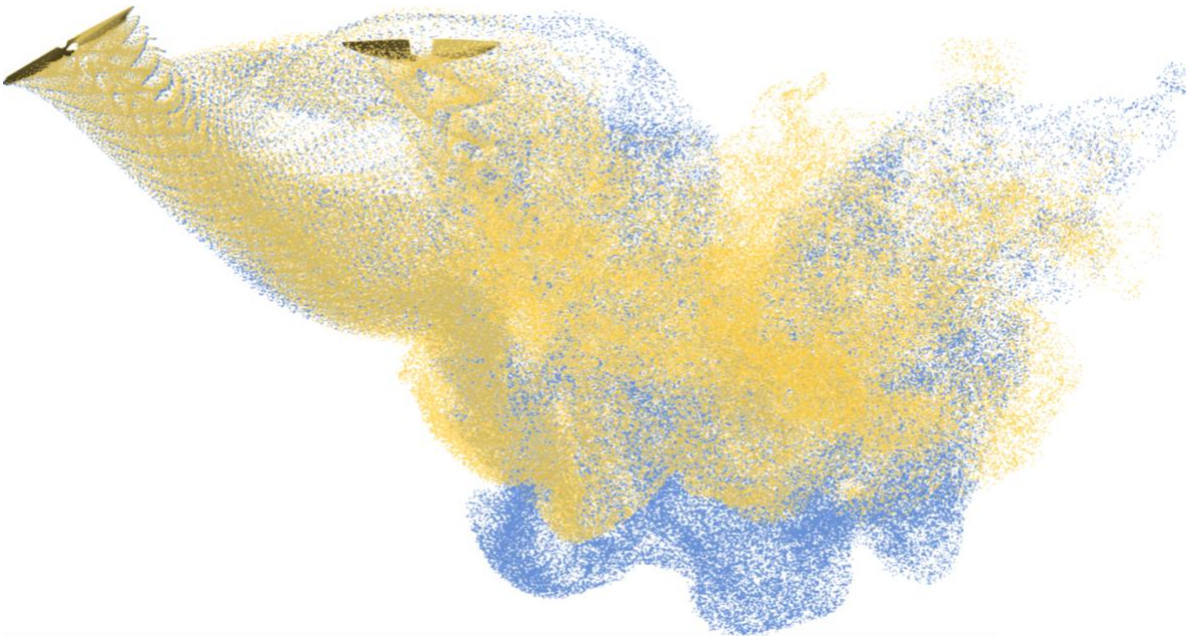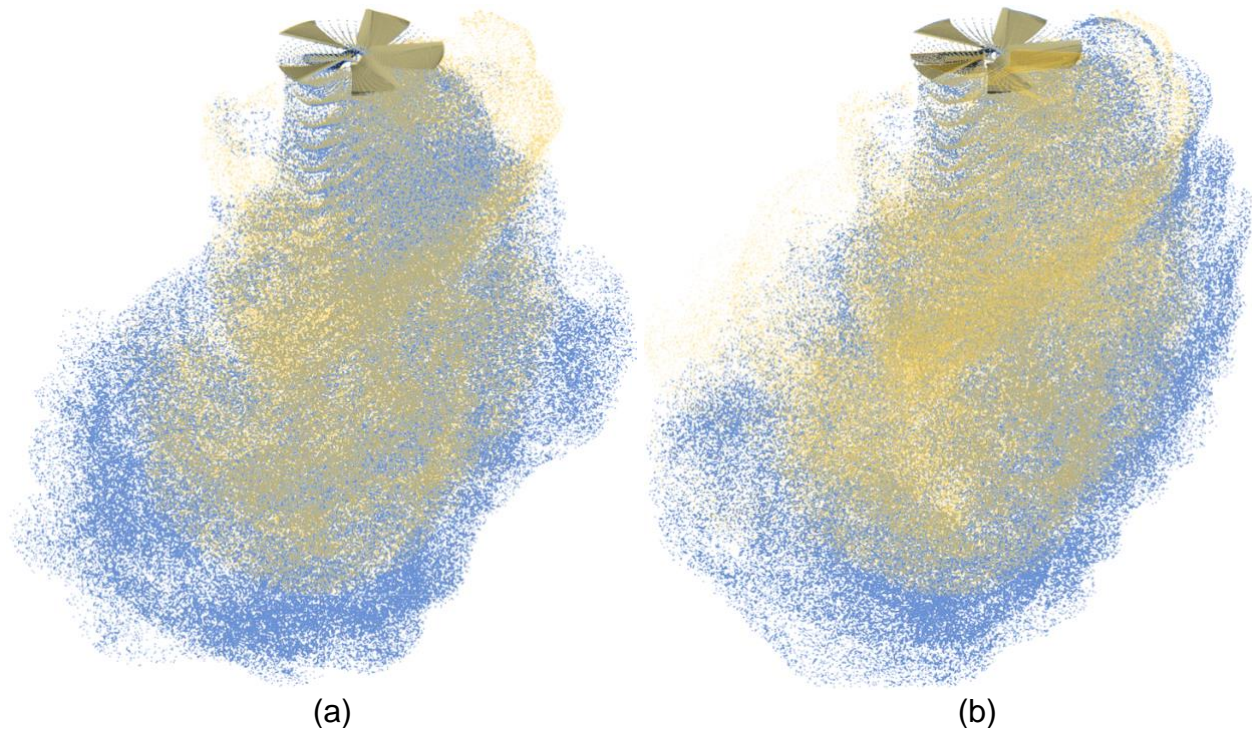Figure 5-4. Qualitative wake comparison between dual rotor system's wake (blue) and isolated rotors' wakes (yellow) at a forward flight case ($\theta_{\text{tilt}} = 60°$ with $U_\infty = 10$ m/s), from a front view. Each point corresponds to a wake particle. The freestream flow is moving into the page. Their rotor offsets differ as follows: (a) offset = 2.5R, (b) offset = 4.5R.

5.2 Thrust Results

Figure 5-5 highlights the coefficient of thrust results in terms of percent error from the isolated cases. Here, we are able to observe how the c_T values from each of the two rotors change as the three controlled variables are adjusted. The first noticeable trend is that the 2-blade rotor's c_T performance is more impacted than the tilter's c_T across all cases. This is expected due to its downstream placement with respect to the front rotor, which makes it more likely to be affected by the tilter's wake, especially in cases with flight conditions involving high free-stream velocities and tilting angles. These effects are generally very negative, as it impacts the aft rotor's thrust significantly. For instance, the lifter rotor's thrust decreases by 6% in the best case scenario, while there is a

decrease by 15% in the worst case scenario (high U_∞ and low θ_{tilt}). It is also possible to

observe that rotor offset does not significantly impacts the 2-blade rotor's coefficient of

thrust in the hover case, as it only seems to play a role in cases with higher U_∞. At $U_\infty =$

10 m/s, lifter's c_T varies up to 5% depending on rotor offset and up to 6.5% depending

on tilt angle. Now, in regards to the 5-blade rotor, tilting angle seems to be the only

factor significantly impacting its c_T value. Having said that, in order to maximize the

thrust of the dual rotor system, different rotor offsets are required for different tilt angles.

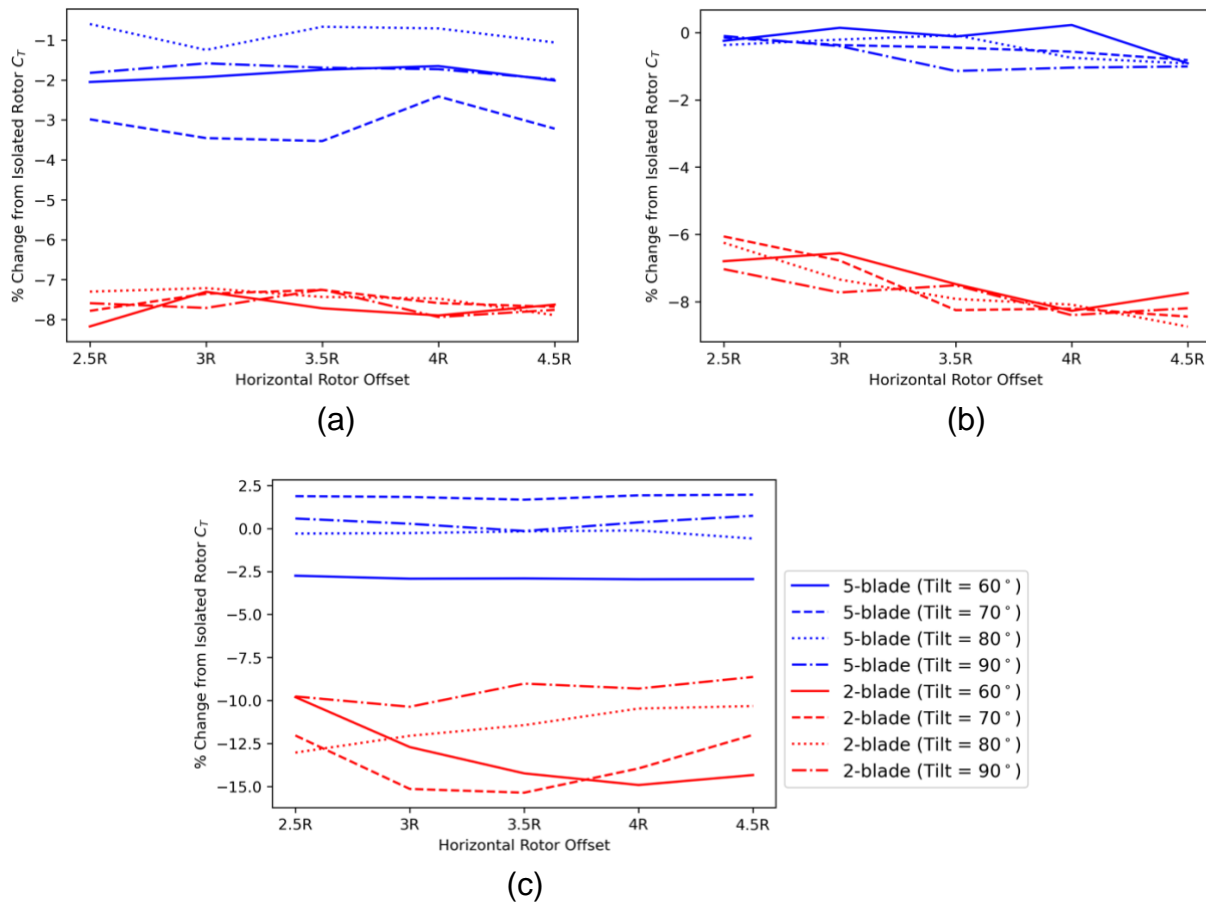Figure 5-5. Percentage change in c_T from isolated rotor cases as a function of rotor offset. Each plot represents a different cruise speed: (a) $U_\infty = 0$ m/s, (b) $U_\infty = 5$ m/s, and (c) $U_\infty = 10$ m/s.

Much like the figure above, Figure 5-6 also presents the resulting coefficient of

thrust values in terms of percent error from the isolated cases. From these plots, we are

42

able to confirm that the tilter's c$_T$ does not depend on rotor offset, as all curves follow

the same trends and paths across the three offsets displayed. Additionally, it is possible

to observe that the 2-blade rotor c$_T$ curves remain fairly constant, except in the cases

involving fight conditions with $U_\infty = 10$ m/s, as shown by the dashed lines. By varying

the tilt angle of the front rotor, the aft rotor's c$_T$ varies up to 7.2% – which occurs when

different flight conditions are combined with certain tilt angles. For instance, the lowest

c$_T$ values recorded at $U_\infty = 0$ m/s, $U_\infty = 5$ m/s, and $U_\infty = 10$ m/s, occurred when $\theta_{tilt} =$

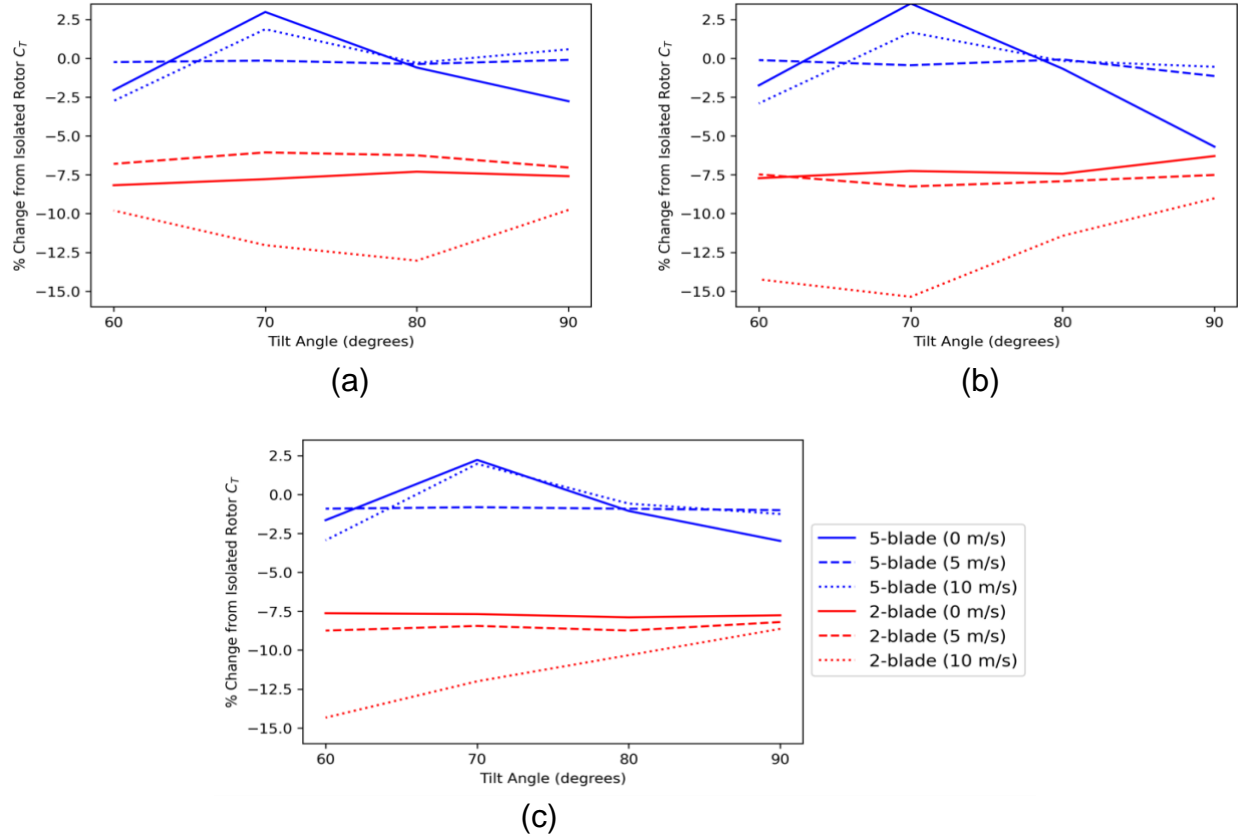80°, $\theta_{tilt} = 70°$, and $\theta_{tilt} = 60°$, respectively.

Figure 5-6. Percentage change in c$_T$ from isolated rotor cases as a function of tilt angle. Each plot represents a different rotor offset: (a) offset $= 2.5R$, (b) offset $= 3.5R$, and (c) offset $= 4.5R$.

5.3 Acoustic Results

Figure 5-7 highlights the changes in SPL at the BPF as a function of tilt angle for each of the four observer locations. Each plot includes nine curves that display the simulation data from the three free-stream velocities combined with three different rotor offsets: $2.5R$, $3.5R$, and $4.5R$. The first trend that is observed is the flat curve behavior on the plots near the rotor plane: Figures 5-7a and 5-7b. This is expected, as the SPL changes in and near the rotor plane are heavily impacted by the thickness loading of the blades, which is dominated by the blade geometry. Therefore, given that the geometry does not change, these values are expected to remain constant among all test cases. Additionally, we are able to observe that U_∞ is a large contributor to the SPL changes observed, as the curves gradually change shape as the free-stream velocity increases. In all four observer locations, the blue curves ($U_\infty = 0$ m/s) vary up to 0.7 dB across all the different cases, while the red curves ($U_\infty = 10$ m/s) vary up to 5.5 dB. Additionally, U_∞ seems to impact the SPL less at lower tilt angles (forward flight configuration). This occurs as no free-stream velocity is needed to move the front rotor's wake into the aft rotor's region, due to the tilting of the front rotor pushing its wake in the lifter's direction.

Much like in the thrust plots previously presented, it is possible to observe from Figure 5-7 that different combinations of U_∞, θ_{tilt}, and rotor offset are needed to obtain the lowest SPL values. For instance, at $\theta_{tilt} = 90°$ and $U_\infty = 10$ m/s, the SPL can be increased by 3.6 dB when lowering the rotor offset from $4.5R$ to $2.5R$. Additionally, a decrease of 7.8 dB in SPL can be observed at the lowest observer when U_∞ is increased from 0 m/s to 10 m/s.
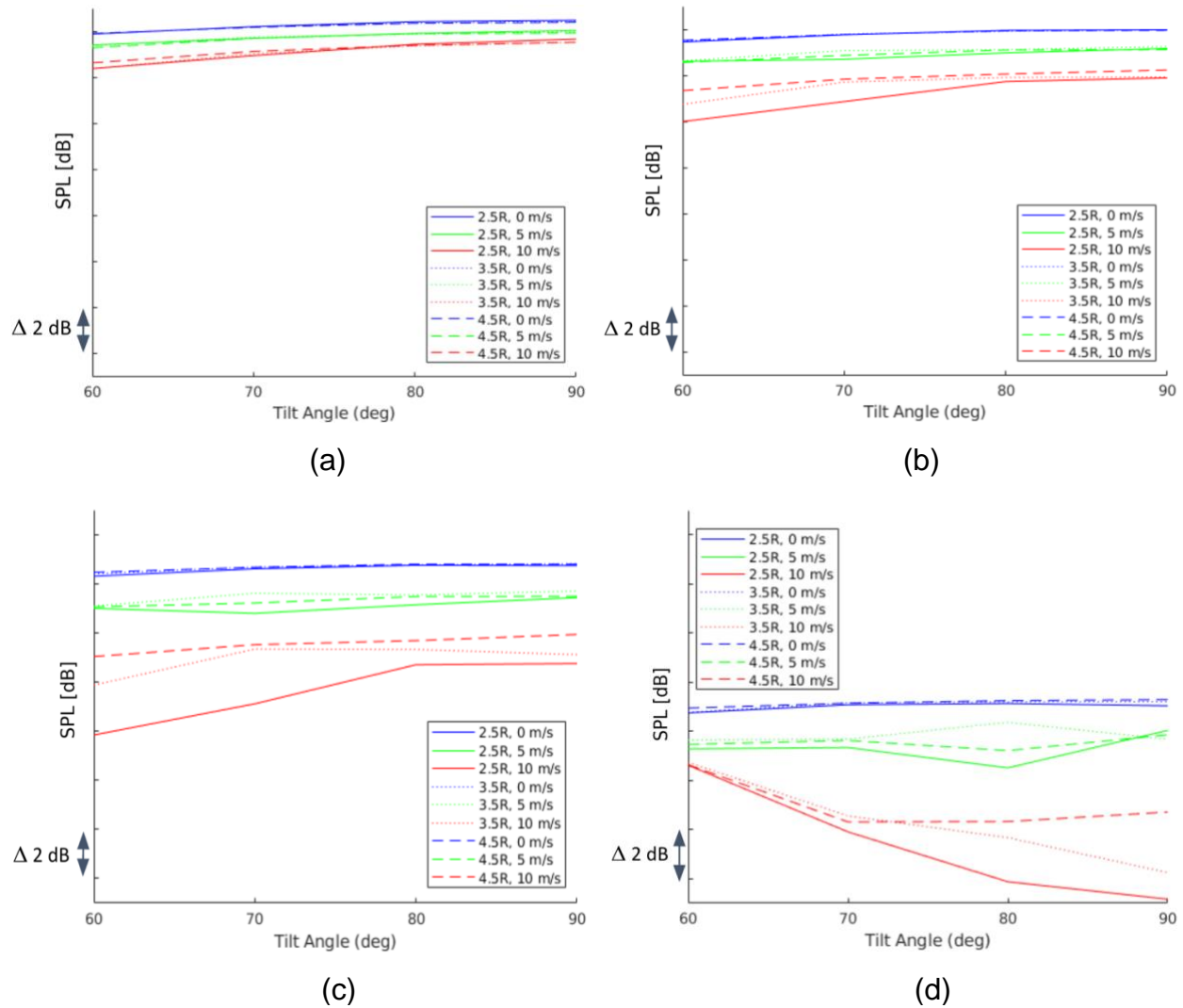
Figure 5-7. Sound pressure level (SPL) at the blade pass frequency (BPF) as a function of tilt angle at each of the four observer locations investigated: (a) Observer #1 (rotor plane), (b) Observer #2 (10° below rotor plane), (c) Observer #3 (20° below rotor plane), and (d) Observer #4 (30° below rotor plane). All y-axes display the same SPL range.

Figure 5-8 is similar to the prior figure, however now, OASPL is investigated. Similarly to SPL, thickness loading is also responsible for the changes in OASPL near the rotor plane, as it is dominated by the blade geometry. On the other hand, OASPL behaves differently across all the cases, as it seems to be hardly affected by any of the controlled variables. Given the similarity between the different curves of the same color, it is possible to deduce that OASPL is invariant with rotor offset, except in lower

observer planes when U_∞ is higher. In this case, it varies slightly, especially at low θ_{tilt}.

Additionally, a decrease of up to 0.6 dB is observed in OASPL when increasing θ_{tilt}

from 60° to 90°. Also, it is important to note that both SPL at the BPF and OASPL are

lowest at $U_\infty = 10$ across all cases. For instance, in comparison to the hover condition,

at 30° below the rotor plane, OASPL is around 4 dB lower, while SPL is 2.5 to 4 dB

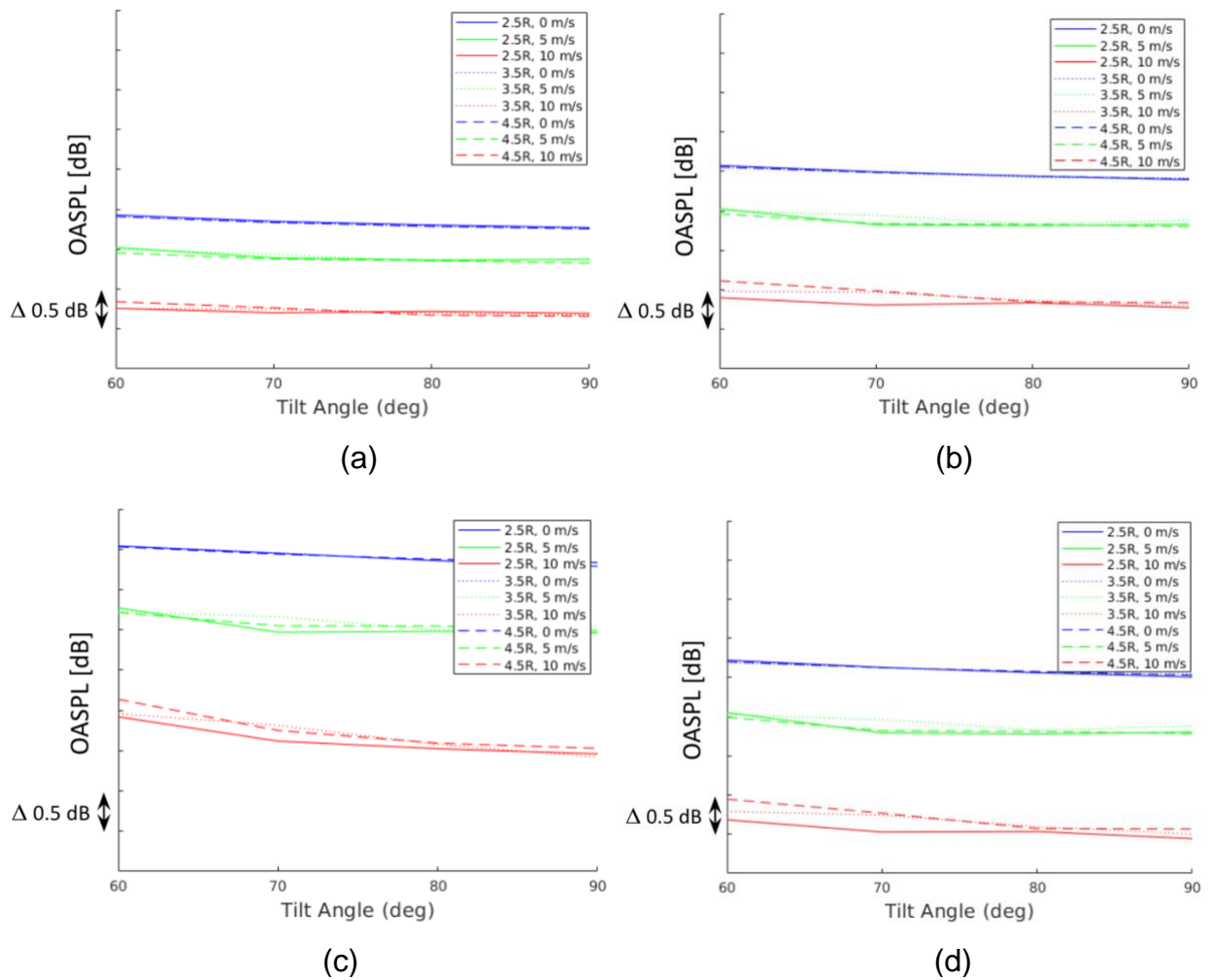lower (depending on θ_{tilt}).

Figure 5-8. Overall sound pressure level (OASPL) as a function of tilt angle at each of the four observer locations investigated: (a) Observer #1 (rotor plane), (b) Observer #2 (10° below rotor plane), (c) Observer #3 (20° below rotor plane), and (d) Observer #4 (30° below rotor plane). All y-axes display the same OASPL range.

CHAPTER 6
CONCLUSIONS AND SCOPE OF FUTURE WORK

The goal of this chapter is to provide a brief summary of the study performed, the results acquired, and the conclusions drawn. The second section of this chapter provides the reader with the scope of future work regarding to this thesis, along with some unanswered questions worth investigating.

6.1 Summary and Conclusions

In summary, this thesis numerically investigated the interaction effects between a pair of sub-scale eVTOL rotors in tandem configuration, and how they affect the rotors' performance. This study examined the effects of adjusting the horizontal spacing, rotor tilt angles, and forward flight conditions. The rotors' performance was characterized by thrust coefficient and acoustic radiation, which was described by the BPF SPL and OASPL. A mid-fidelity computational fluid dynamics solver, called DUST, was used to predict the aerodynamic flow-field. The total tonal acoustic pressure at certain observer locations was predicted using an acoustic solver based on the Farassat 1A solution of the Ffowcs-Williams and Hawkings equation utilizing the aerodynamic flow-field. This method was validated via experimental measurement.

The performance of the rotors in the tandem configuration was compared to the performance of isolated rotors in the same flight conditions, in order to highlight any interactive effects. The following are the main findings and conclusions drawn from this study:

- The mid-fidelity tool employed, DUST, is a valuable tool for similar studies, and preliminary design. An observed limitation was its accuracy in high free-stream velocity cases.

- The tilter rotor's thrust is primarily impacted by the tilt angle; adjusting this may result in a $\pm$ 3.5% change C_T.

- Under low cruise speeds, the lifter rotor's C$_T$ only varies under low tilt angles, due to its interaction with the wake from the front rotor.

- To maximize thrust from both rotors, different rotor offsets are required for different tilt angles and free-stream velocities.

- The system's BPF SPL is primarily affected by cruise speed and tilt angle, as rotor offset only plays a role in high U_∞ and high θ_{tilt} conditions.

- Little change is observed to both SPL and OASPL at hover conditions when varying rotor offset and θ_{tilt}.

- OASPL varies little with different tilt angles, but it does not vary with rotor offset and U_∞.

These results have the potential to bring significant benefits to the field, as they can aid designers in the development of more efficient and quieter eVTOL vehicles, leading to a safer and more sustainable mode of transportation. By providing valuable insights into the underlying mechanisms that govern rotor interactions, these studies can help engineers better design these vehicles by improving their performance while lowering any radiated noise. These results may also aid in the development of advanced design tools and optimization methods that consider rotor-rotor interaction effects. Overall, this work has significant potential to advance developments surrounding this transformative technology, which may help pave the way for its widespread adoption.

6.2 Scope of Future Work

Based on the presented study, the following questions still remain unanswered and may serve as guidance to extend the work in this field:

- How is the noise radiated by the rotors impacted when varying the different controlled variables while keeping the rotors' thrust constant? This is important as vehicles will need to maintain certain levels of thrust during their flights. This can be done by actively varying the rotors' RPMs and the blades' collective angles.

- In this work, the rotation rate of both rotors was the same, and was kept constant throughout the simulations. Additionally, both rotors rotated in the same direction. Hence, how do different RPMs change the interaction effects between the two rotors? Do rotors spinning in opposite directions create any beneficial effects on their performance? These critical questions have been explored extensively for helicopter configurations, but not complex eVTOL configurations.

- In this study, we only analyzed a system involving two rotors. How would adding a body between them, such as a wing, impact the way they interact? Could that stop the front rotor's wake from going into the aft rotor's inlet region?

- Given that only a pair of rotors in tandem were investigated in this study, the effect of side-by-side rotors on the pair of rotors in tandem was not explored. How do front side-by-side rotors interact with the aft rotors? Is there an ideal configuration of front rotors that minimizes interactive effects going downstream?

- Could a vertical offset between the two rotors help avoid interaction between their wakes? Should the aft rotor be placed over the front rotor in order to avoid pulling the turbulent wake through its blades?

These are the questions that the author of this thesis wishes to continue to investigate moving forward. A single study could explore a combination of these questions, which may be of great importance to engineers and designers in the near future. Urban air mobility and eVTOL are expected to be widely available in the next decades, therefore this field of research has and will experience high demand in the next few years.

LIST OF REFERENCES

[1]   N. Polaczyk, E. Trombino, D. P. Wei, and D. M. Mitici, "A Review of Current Technology and Research in Urban On-Demand Air Mobility Applications," in *8th Biennial Autonomous VTOL Technical Meeting and 6th Annual Electric VTOL Symposium 2019*, Mesa, AZ, Jan. 2019. [Online]. Available: http://resolver.tudelft.nl/uuid:10d1c68a-dfb9-4419-a912-26e6c1742853

[2]   I. Greenfeld, "Concept of Operations for Urban Air Mobility Command and Control Communications," NASA Glenn Research Center Cleveland, OH, NASA/TM-2019-220159, Apr. 2019.

[3]   Z. (Henry) Jia and S. Lee, "High-Fidelity Computational Analysis on the Noise of a Side-by-Side Hybrid VTOL Aircraft," *j am helicopter soc*, vol. 67, no. 2, pp. 1–14, Apr. 2022, doi: 10.4050/JAHS.67.022005.

[4]   "Archer." https://www.archer.com/ (accessed Jan. 24, 2023).

[5]   "Joby Aviation | Joby." https://www.jobyaviation.com/ (accessed Jan. 24, 2023).

[6]   "Lilium Air Mobility - Lilium." https://lilium.com/ (accessed Jan. 24, 2023).

[7]   "Acubed - We are the Silicon Valley innovation center of Airbus." https://acubed.airbus.com/ (accessed Jan. 24, 2023).

[8]   H. H. Hubbard, *Aeroacoustics of Flight Vehicles: Theory and Practice. Volume 1: Noise Sources*, vol. 1. National Aeronautics and Space Administration Langley Research Center, Hampton, VA, Aug. 1991.

[9]   R. Healy, M. Misiorowski, and F. Gandhi, "A CFD-Based Examination of Rotor-Rotor Separation Effects on Interactional Aerodynamics for eVTOL Aircraft," *Journal of the American Helicopter Society,* vol. 67, no. 1, pp. 1–12, Jan. 2022, doi: 10.4050/JAHS.67.012006.

[10]   M. Misiorowski, F. Gandhi, and A. A. Oberai, "Computational Study on Rotor Interactional Effects for a Quadcopter in Edgewise Flight," in IEEE Aerospace Conference Proceedings, Big Sky, MT, Mar. 2018, pp. 1-11.

[11]   R. Duivenvoorden, M. Voskuijl, and L. Moree, "Numerical and Experimental Investigation into the Aerodynamic Benefits of Rotorcraft Formation Flight," Journal of the American Helicopter Society, vol. 67, no. 1, Jan. 2022, pp. 1-15.

[12]   L. Cambier, S. Heib, and S. Plot, "The Onera *elsA* CFD software: input from research and feedback from industry," *Mechanics & Industry*, vol. 14, no. 3, pp. 159–174, 2013, doi: 10.1051/meca/2013056.

[13] N. Kroll and J. K. Fassbender, Eds., "MEGAFLOW - Numerical Flow Simulation for Aircraft Design: Results of the second phase of the German CFD initiative MEGAFLOW," DLR symposium, Braunschweig, Germany, Dec. 2005.

[14] M. Biava, M. Woodgate, and G. N. Barakos, "Fully Implicit Discrete-Adjoint Methods for Rotorcraft Applications," *AIAA Journal*, vol. 54, no. 2, pp. 735–749, Feb. 2016, doi: 10.2514/1.J054006.

[15] R. Piccinini, M. Tugnoli, and A. Zanotti, "Numerical Investigation of the Rotor-Rotor Aerodynamic Interaction for eVTOL Aircraft Configurations," *Energies*, vol. 13, Nov. 2020, doi: 10.3390/en13225995.

[16] J. Yin and S. Ahmed, "Aerodynamics and aeroacoustics of helicopter main-rotor/tail-rotor interaction," in *5th AIAA/CEAS Aeroacoustics Conference and Exhibit*, Bellevue, WA, May 1999. doi: 10.2514/6.1999-1929.

[17] G.-H. Cottet and P. D. Koumoutsakos, *Vortex Methods: Theory and Practice*, 1st ed. Cambridge University Press, 2000. doi: 10.1017/CBO9780511526442.

[18] M. Wentrup *et al.*, "An overview of DLR compound rotorcraft aerodynamics and aeroacoustics activities within the CleanSky2 NACOR Project," in *AHS Forum 2018*, Phoenix, AZ, United States, May 2018.

[19] A. Zanotti, A. Savino, M. Palazzi, M. Tugnoli, and V. Muscarello, "Assessment of a Mid-Fidelity Numerical Approach for the Investigation of Tiltrotor Aerodynamics," *Applied Sciences*, vol. 11, no. 8, p. 3385, Apr. 2021, doi: 10.3390/app11083385.

[20] M. sTool," presented at the VFS Aeromechanics for Advanced Vertical Flight Technical Meeting, San Jose, CA, Jan. 2020.

[21] K. Lindsay and R. Krasny, "A Particle Method and Adaptive Treecode for Vortex Sheet Motion in Three-Dimensional Flow," *Journal of Computational Physics*, vol. 172, no. 2, pp. 879–907, Sep. 2001, doi: 10.1006/jcph.2001.6862.

[22] D. Montagnani, M. Tugnoli, F. Fonte, A. Zanotti, M. Syal, and G. Droandi, "Mid-Fidelity Analysis of Unsteady Interactional Aerodynamics of Complex VTOL Configurations," presented at the 45th European Rotorcraft Forum, Warsaw, Poland, Sep. 2019.

[23] F. Farassat, "Derivation of Formulations 1 and 1A of Farassat," Technical Report No. NASA/TM-2007-214853, National Aeronautics and Space Administration, Langley Research Center, Hampton, VA, Mar. 2007.

[24] J. E. Ffowcs Williams and D. L. Hawkings, "Sound generation by turbulence and surfaces in arbitrary motion," *Phil. Trans. R. Soc. Lond. A*, vol. 264, no. 1151, pp. 321–342, May 1969, doi: 10.1098/rsta.1969.0031.

[25] R. Brentner, "An efficient and robust method for predicting helicopter rotor high-speed impulsive noise," AIAA, 34th Aerospace Sciences Meeting and Exhibit, Reno, NV, Jan. 1996, doi: 10.2514/6.1996-151.

[26] J. Goldschmidt, H. Tingle, P. Ifju, S. A. E. Miller, L. Ukeiley, B. Goldman, G. Droandi, and K. Lee, "Acoustics and Forces from Isolated and Installed Tandem eVTOL Rotor Configurations," AIAA SciTech, National Harbor, MD, Jan. 23-27, AIAA 2023-0791, 2023. doi: 10.2514/6.2023-0791

BIOGRAPHICAL SKETCH

Gustavo is an international graduate student from Brazil who defended his master's thesis in March 2023, and he is planning to graduate with a Master of Science degree in aerospace engineering with a focus in thermal science and fluid dynamics (TSFD) from the University of Florida. Before moving to Florida, Gustavo spent four years pursuing double Bachelor of Science degrees in Mechanical Engineering and Aerospace Science and Engineering at the University of California, Davis. By combining all the experience he has gathered from his courses, research, clubs, and personal projects, Gustavo hopes to be involved in engineering projects that can impact people's lives for the better, specifically in the field of aerodynamics and acoustics.

Gustavo's hobbies include playing football (soccer), riding his long board, as well as designing, building, and flying remote controlled planes and quadcopters. He hopes to one day competitively participate in drone races all across the world.